Supporting Information for Metal-Ligand Cooperativity of a Co–P Moiety

*Seji Kim and Yunho Lee**

Department of Chemistry, Korea Advanced Institute of Science and Technology
Daejeon 34141, Republic of Korea

Contents

Experimental Section.

Figure S1. ^{1}H NMR spectrum of $(P_2P–PP_2)(CoBr)_2$ (**1-Br**) in benzene-d_6 at room temperature.

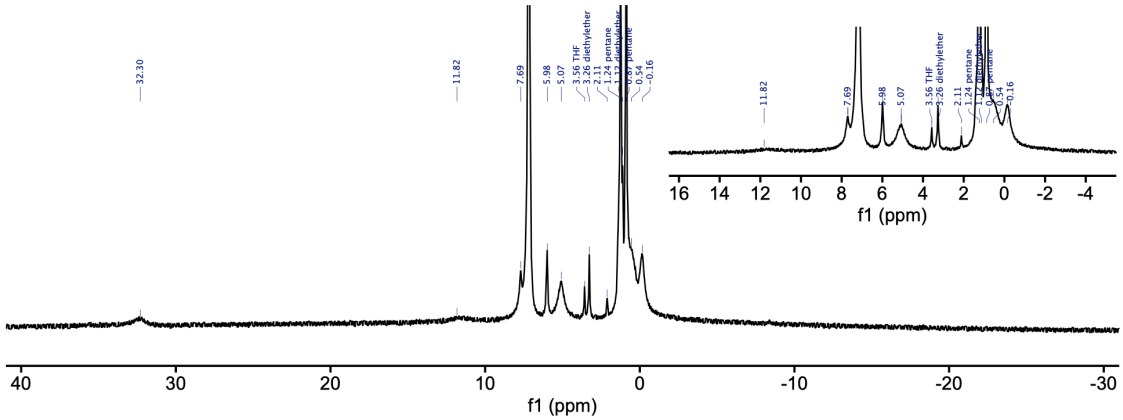

Figure S2. ^{1}H NMR spectrum of $(PP^{H}P)CoBr_2$ (**2**) in benzene-d_6 at room temperature.

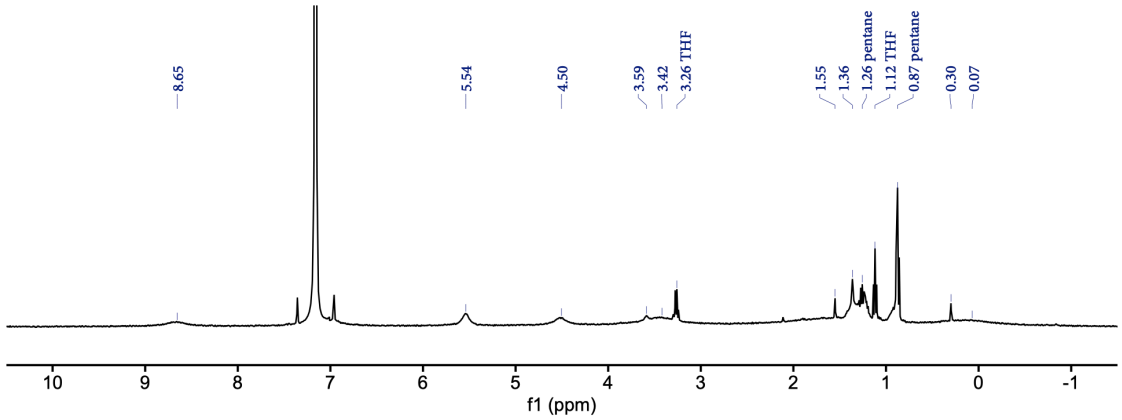

Figure S3. ^{1}H NMR spectrum of $\{(\mu\text{-}PP_2)Co\}_2$ (**3**) in benzene-d_6 at room temperature.

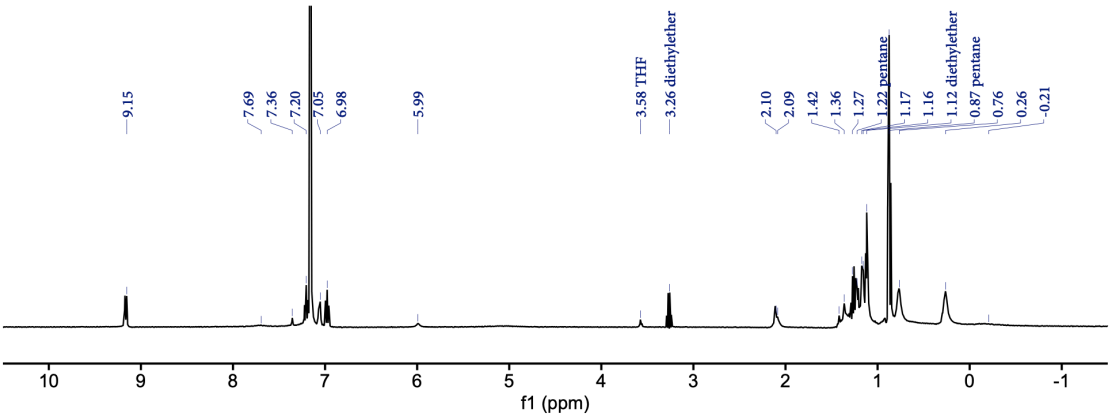

Figure S4. ^{1}H NMR spectrum of $\{(P_2P–PP_2)Co(OTf)\}_2$ (**1-OTf**) in benzene-d_6 at room temperature.

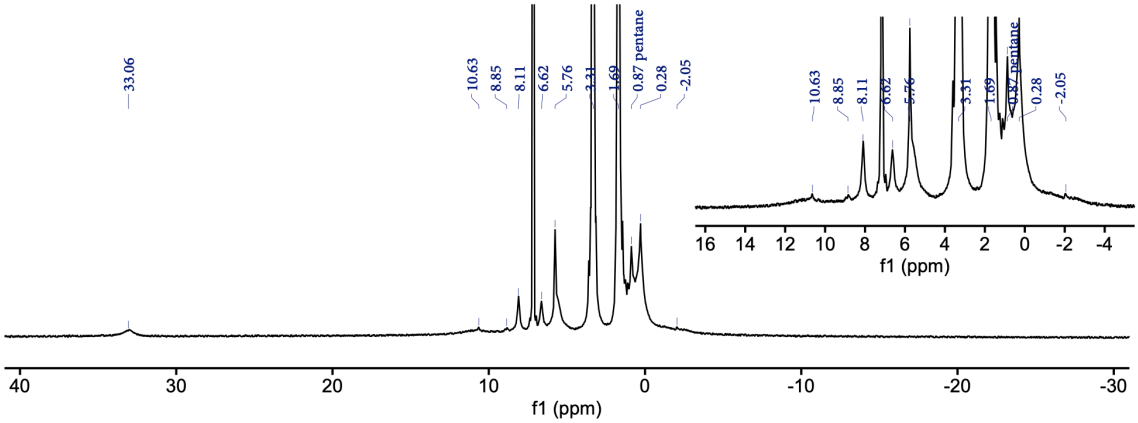

Figure S5. ^{1}H NMR spectrum of $(P_2P–PP_2)\{Co(OPh)\}_2$ (**1-OPh**) in benzene-d_6 at room temperature.

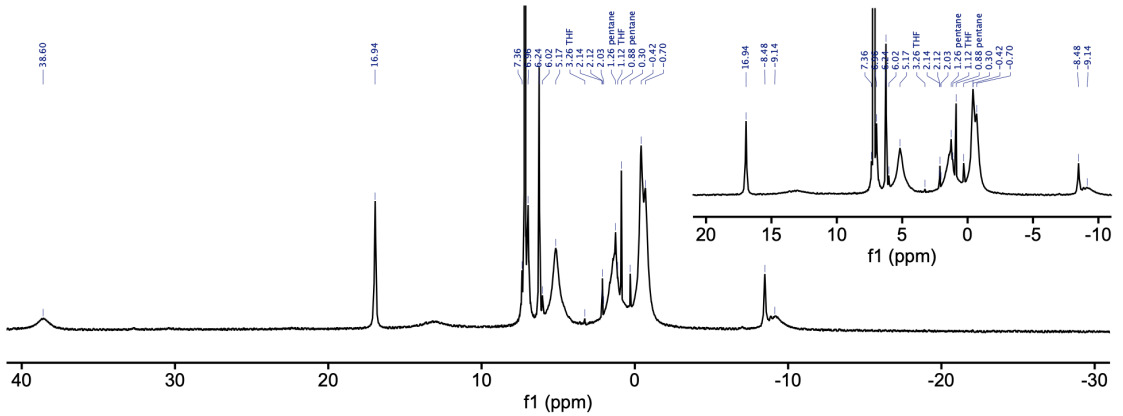

Figure S6. ^{1}H NMR spectrum of ($PP^{OAr}P$)CoBr (**4-Br**) in benzene-d_6 at room temperature.

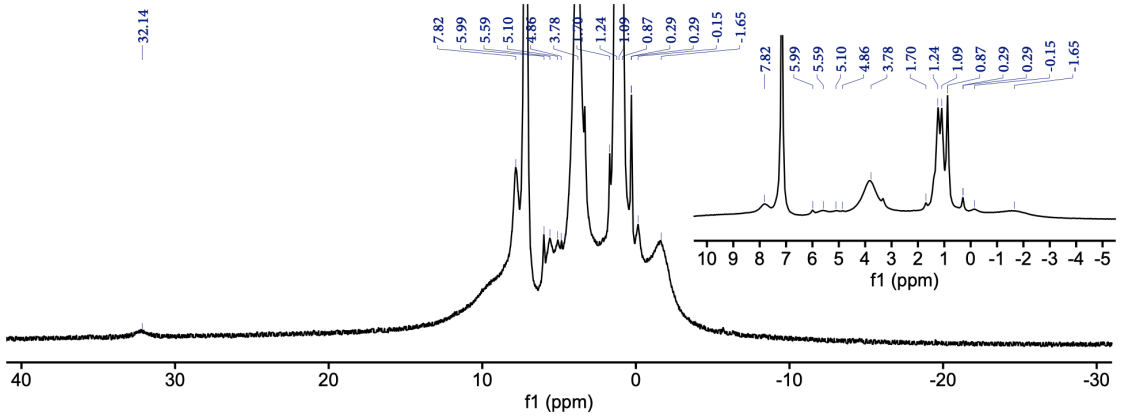

Figure S7. ^{1}H NMR spectrum of (PP^{OAr}P)Co(OPh) (**4-OPh**) in benzene-d_6 at room temperature.

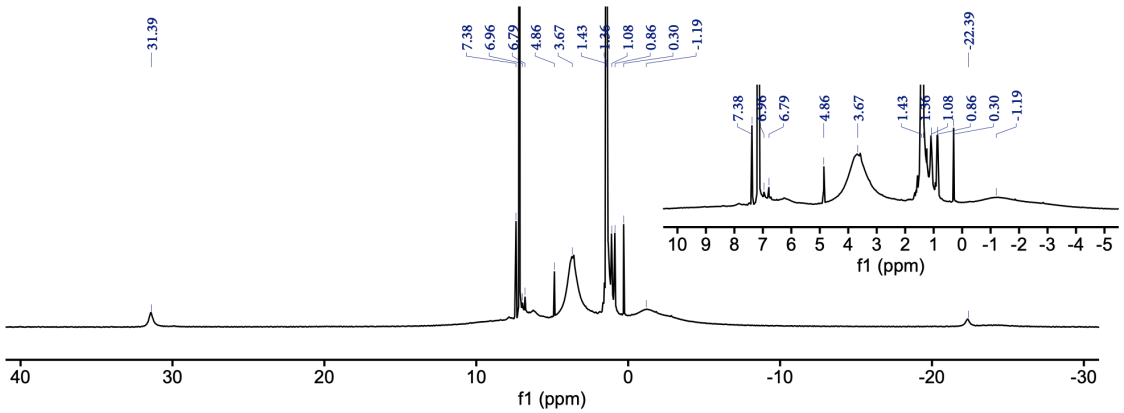

Figure S8. ^{1}H NMR spectrum of (PPP)Co(CN^{t}Bu)$_2$ (**5**) in benzene-d_6 at room temperature.

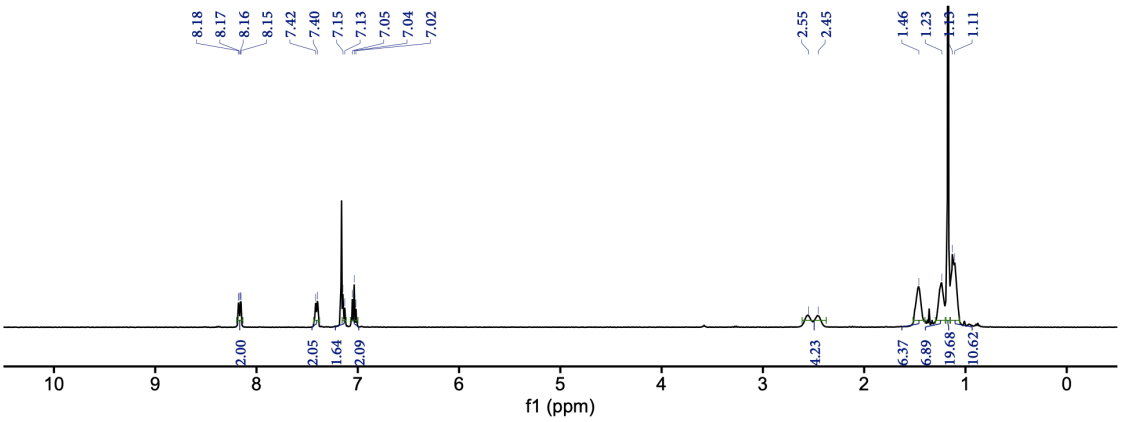

Figure S9. ^{31}P NMR spectrum of (PPP)Co(CN^{t}Bu)$_2$ (**5**) in benzene-d_6 at room temperature.

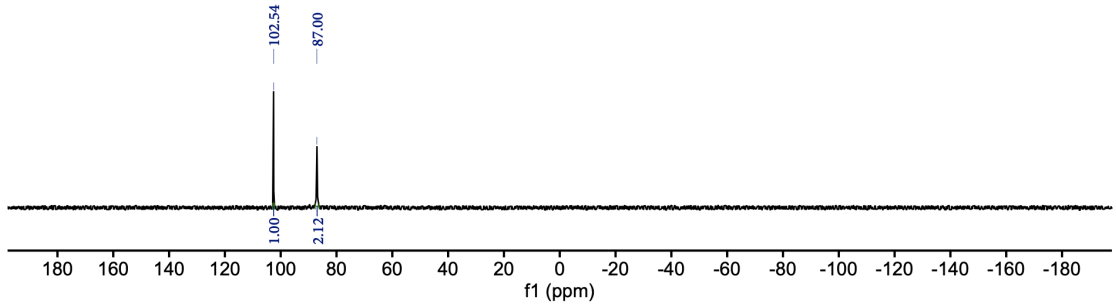

Figure S10. ^{13}C NMR spectrum of (PPP)Co(CN^{t}Bu)$_2$ (**5**) in benzene-d_6 at room temperature.

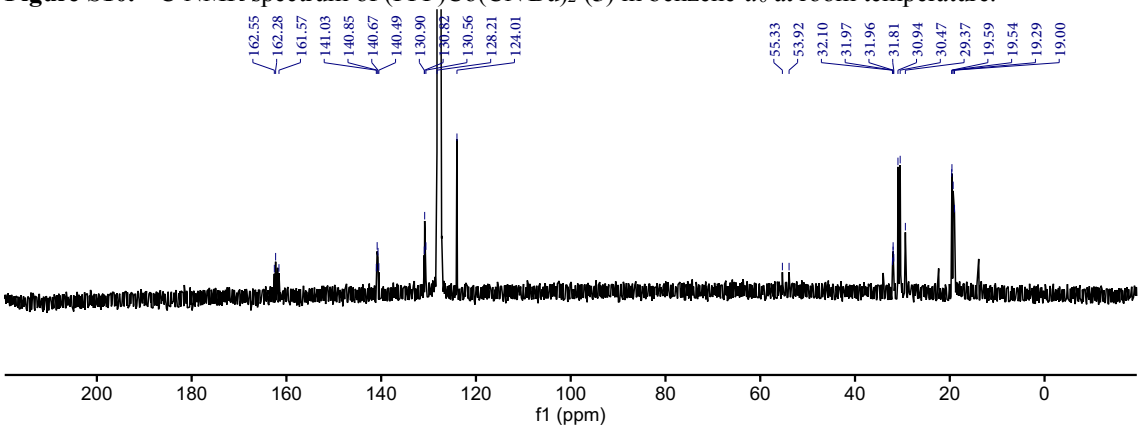

Figure S11. ^{1}H NMR spectrum of (PP^{OPh}P)Co(OPh) (**6**) in benzene-d_6 at room temperature.

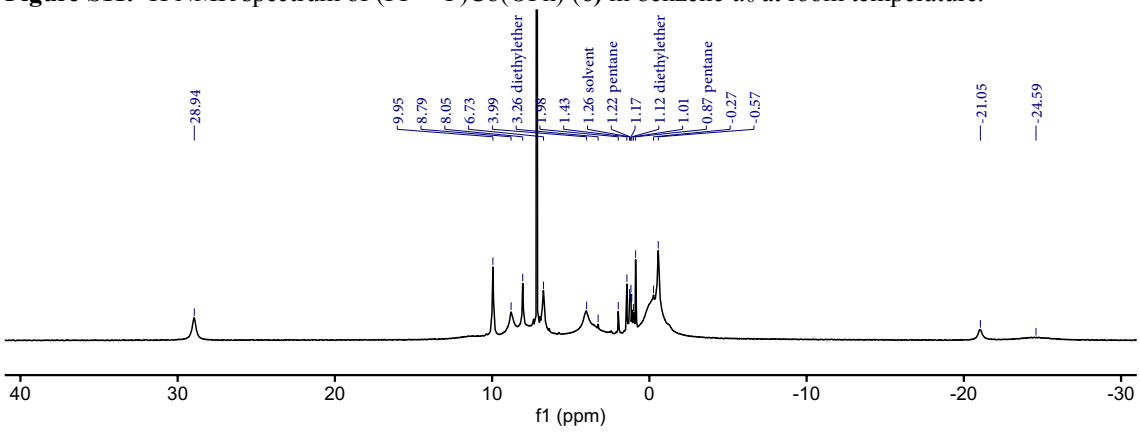

Figure S12. ^{1}H NMR spectrum of {(PPP)Co(CN^{t}Bu)}$_2$ (**7**) in benzene-d_6 at room temperature.

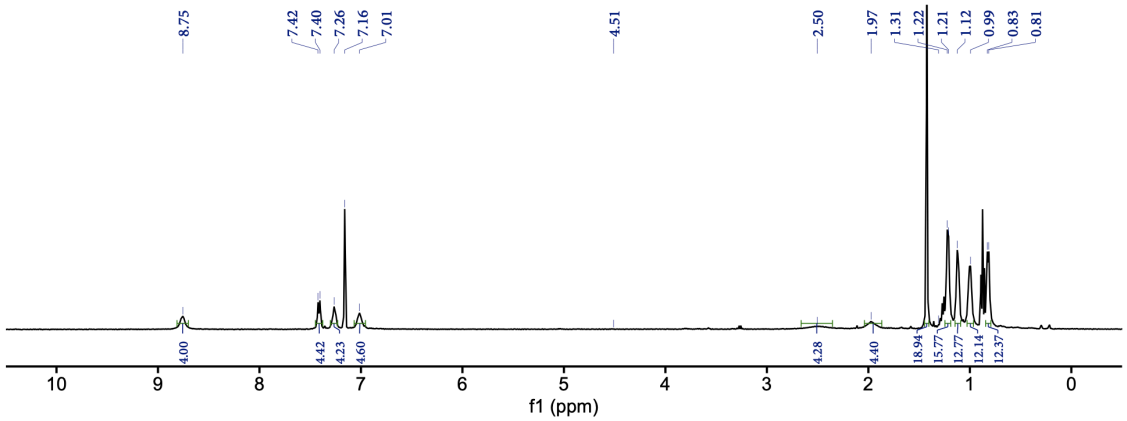

Figure S13. ^{31}P NMR spectrum of {(PPP)Co(CN^{t}Bu)}$_2$ (**7**) in benzene-d_6 at room temperature.

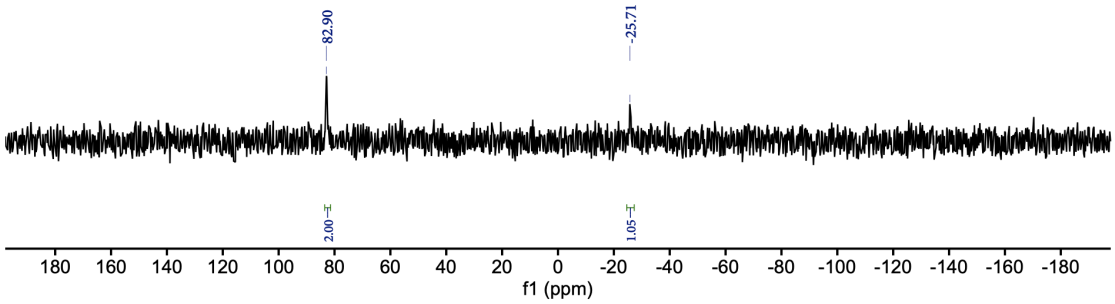

Figure S14. ^{1}H NMR spectra of a mixture of {(μ-PP$_2$)Co}$_2$ (**3**) and (PP^{OPh}P)Co(OPh) (**6**) (a) after 5 min at room temperature and (b) after 2 h heating at 100 °C in acetonitrile-d_3.

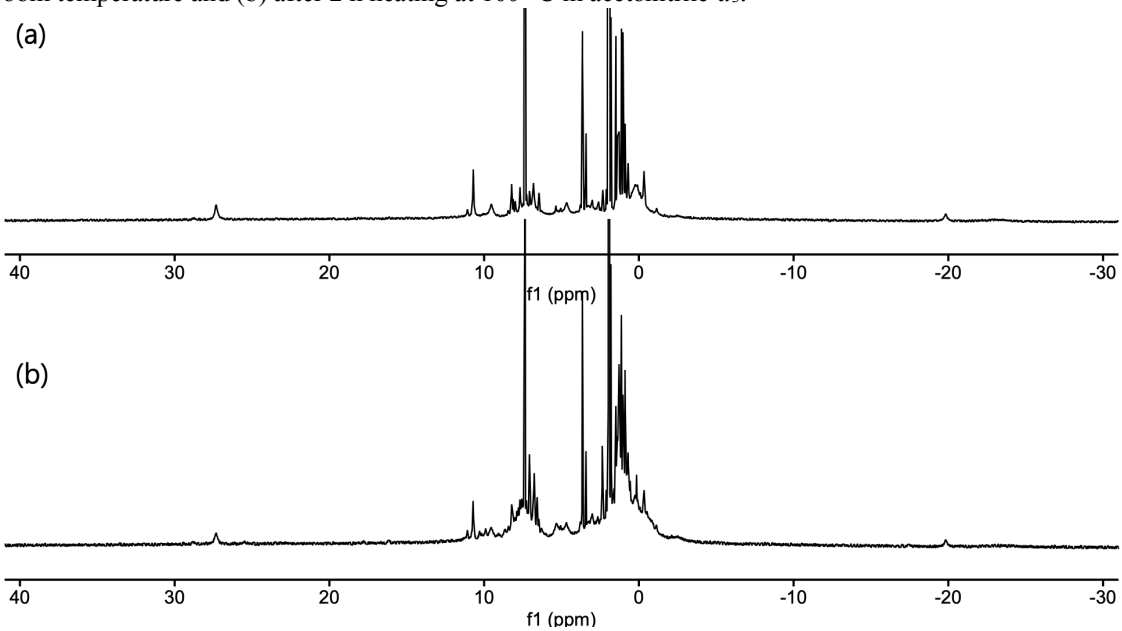

Figure S15. ^{1}H NMR spectra of (a) (P_2P–PP_2){Co(OPh)}$_2$ (**1-OPh**) after stirring 24 h in 6 mL CD_3CN (black) , (b) the isolated diethyl ether-soluble portion of the resulting solution (black) with **1-OPh** (red) and **6** (blue) and (c) the isolated diethyl ether-insoluble powder (black) with **3** (orange) in benzene-d_6 at room temperature.

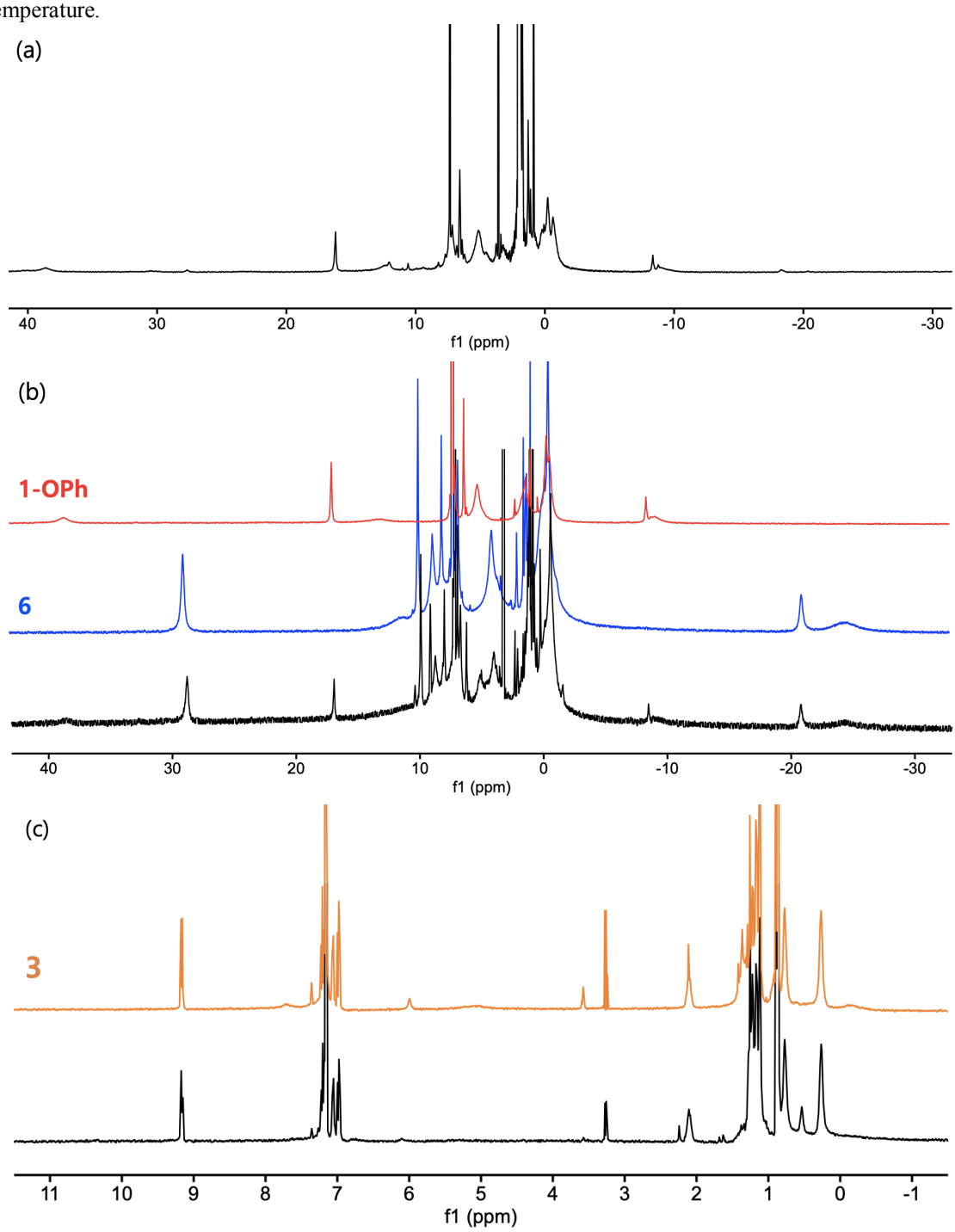

Figure S16. ^{1}H NMR spectra of (a) {(PPP)Co(CN^{t}Bu)}$_2$ (**7**), (b) after 1.5 h and (c) 24 hour heating at 100 °C with two equivalents of ^{t}BuNC and (d) (PPP)Co(CN*t*Bu)$_2$ (**5**) in benzene-d_6 at room temperature.

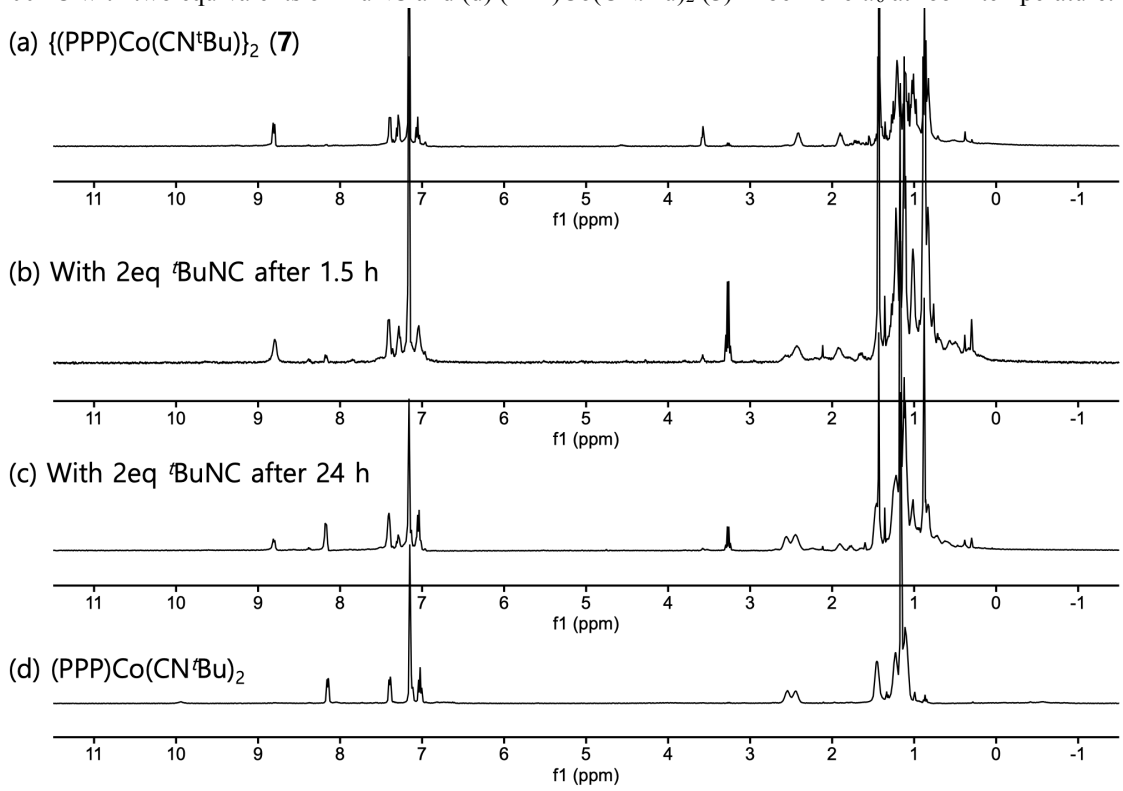

Figure S17. VT ^{1}H NMR spectra profile of (P_2P–PP_2)$(CoBr)_2$ (**1-Br**) in toluene-d_8.

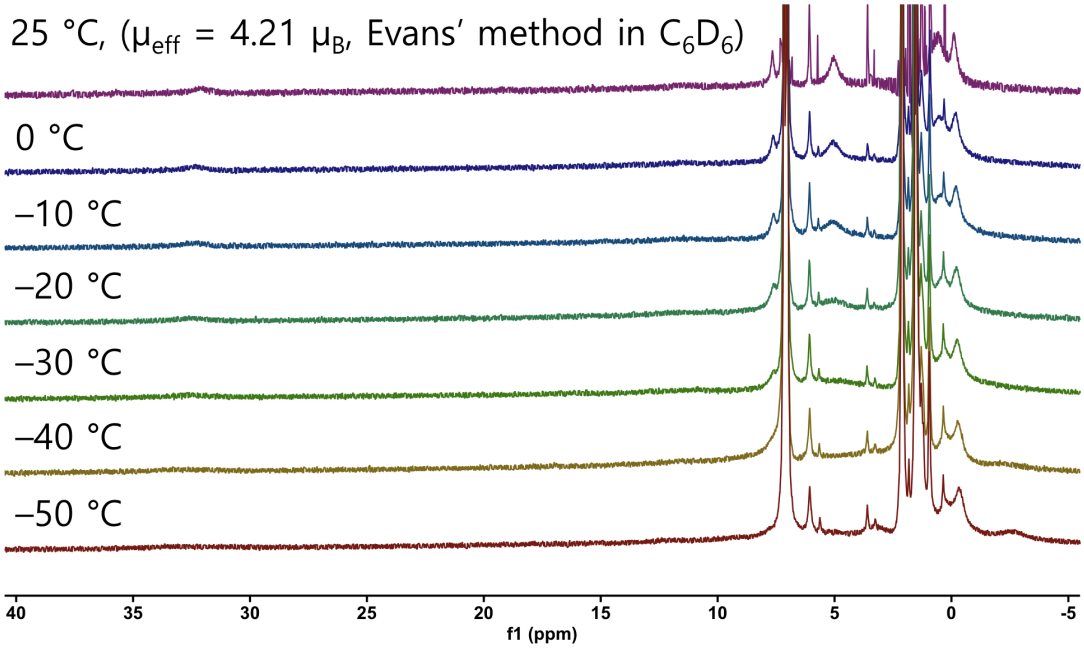

Figure S18. VT ^{1}H NMR spectra profile of {(μ-PP_2)Co}$_2$ (**3**) in toluene-d_8.

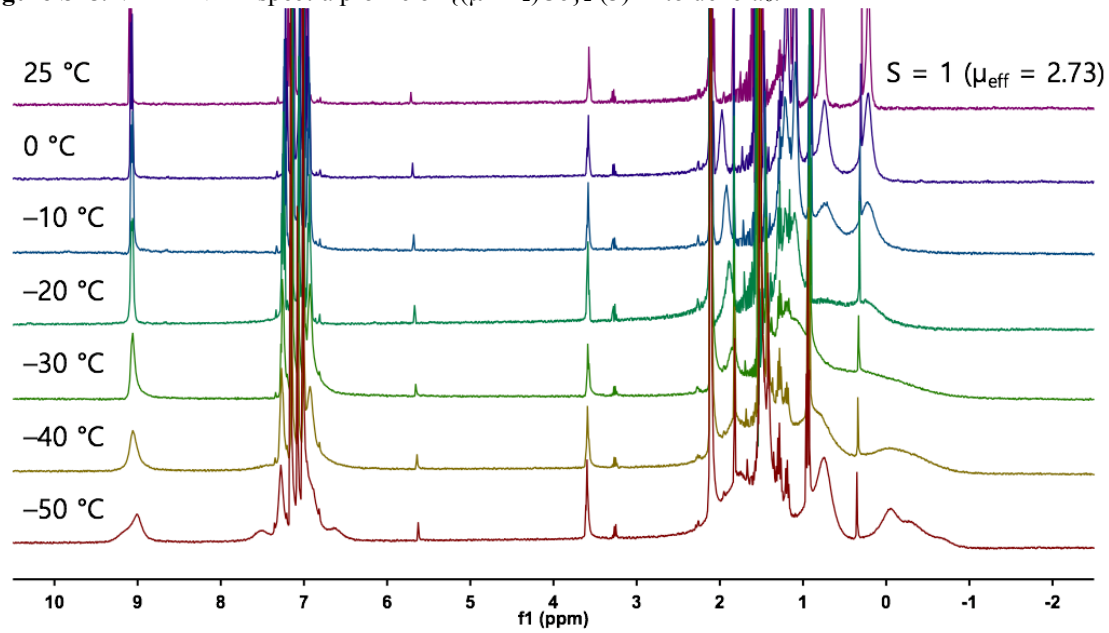

Figure S19. Experimental (black line) X-band EPR spectra of (a) (P_2P–PP_2)($CoBr)_2$ (**1-Br**) in toluene at 10 K and (b) after the irradiation of **1-Br** with a white LED exposure in toluene at room temperature, collected at 10 K.

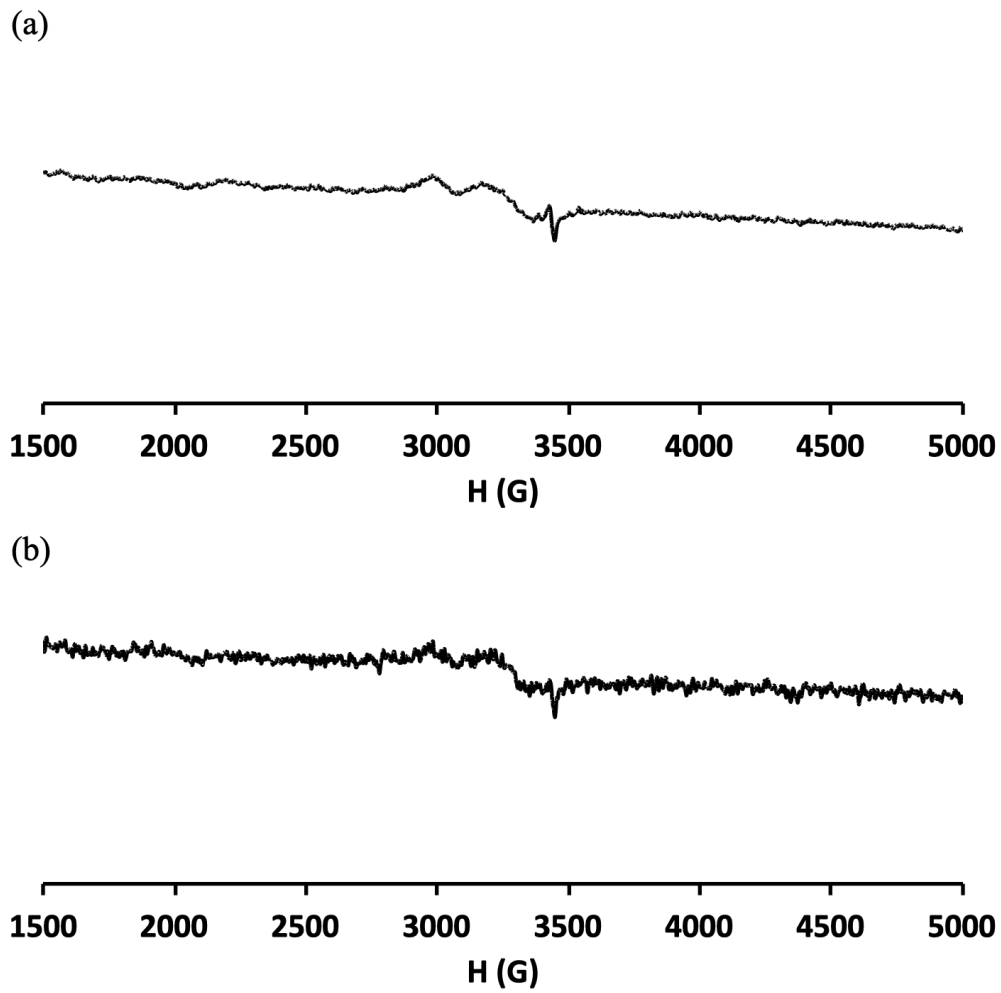

Figure S20. Experimental (black line) and simulated (dashed red line) X-band EPR spectra of ($PP^{H}P$)$CoBr_2$ (**2**) in toluene at 20 K.

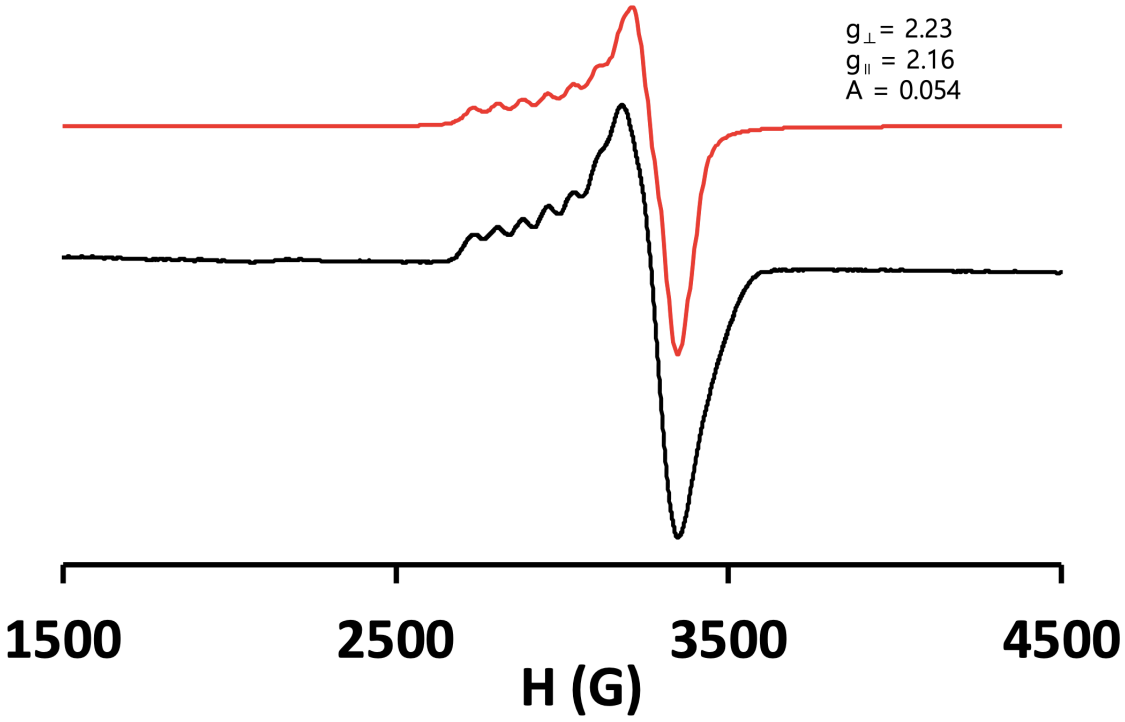

Figure S21. Solid-state structure of (P_2P-PP_2)($CoBr)_2$ (**1-Br**). Hydrogen atoms are omitted for clarity.

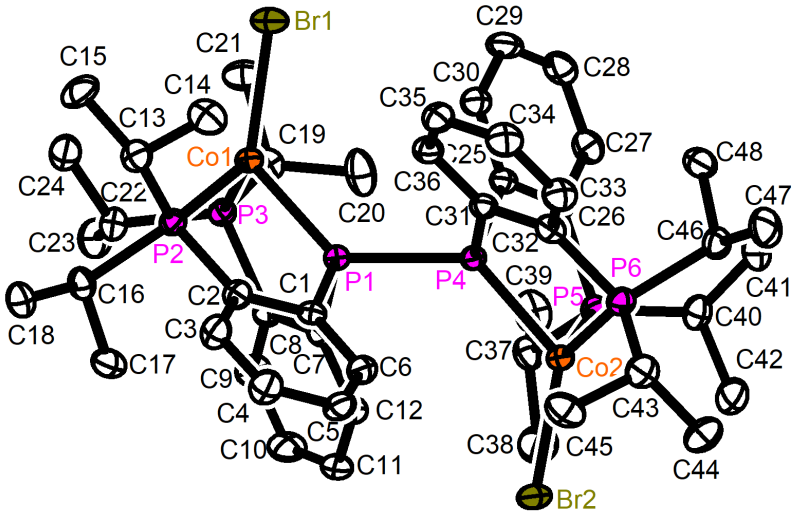

Table S1. Selected bond distances and angles for (P_2P-PP_2)($CoBr)_2$ (Å and °).

Distance	(P_2P–PP_2)($CoBr)_2$	Angle	(P_2P–PP_2)($CoBr)_2$
$d_{P1–P4}$	2.279(2)	∠Co1-P1-P4 ∠Co2-P4-P1	132.22(9) 130.57(9)
$d_{Co1–Br1}$ $d_{Co2–Br2}$	2.352(1) 2.353 (1)	∠Br1-Co1-P1 ∠Br2-Co2-P4	128.15(6) 127.83(6)
$d_{Co1–P1}$ $d_{Co2–P4}$	2.199(2) 2.203(2)	∠P2-Co1-P1 ∠P3-Co1-P1 ∠P5-Co2-P4 ∠P6-Co2-P4	86.30(7) 88.63(7) 86.92(7) 86.46(7)
$d_{Co1–P2}$ $d_{Co1–P3}$	2.257 (2) 2.246 (2)	∠Br1-Co1-P2 ∠Br1-Co1-P3 ∠Br2-Co2-P5 ∠Br2-Co2-P6	117.77(6) 119.43(6) 118.32(6) 114.78(6)
$d_{Co2–P5}$ $d_{Co2–P6}$	2.256(2) 2.250 (2)	∠P2-Co1-P3 ∠P5-Co2-P6	109.66(7) 116.72(7)

Figure S22. Solid-state structure of (PP^HP)$CoBr_2$ (**2**). Hydrogen atoms are omitted for clarity except H1.

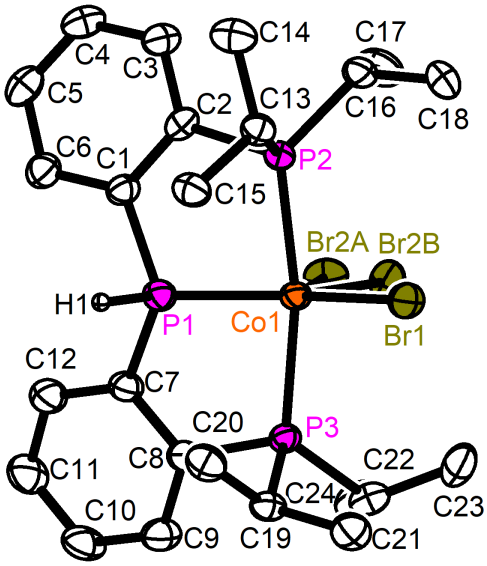

Table S2. Selected bond distances and angles for (PP^HP)$CoBr_2$ (Å and °).

Distance	(PP^HP)$CoBr_2$	Angle	(PP^HP)$CoBr_2$
d_{P1-H1}	1.4086(?)	∠P1-Co1-P2	84.37(4)
$d_{Co1-Br2A}$	2.4805(6)	∠P1-Co1-P3	85.10(4)
$d_{Co1-Br2B}$	2.797(8)	∠P2-Co1-P3	169.31(4)
d_{Co1-P1}	2.145(1)	∠Br1-Co1-P1	143.66(4)
d_{Co1-P2}	2.2284(9)	∠Br1-Co1-P2	90.84(3)
d_{Co1-P3}	2.2481(9)	∠Br1-Co1-P3	96.56(3)
$d_{Co1-Br1}$	2.3742(5)	∠Br2A-Co1-Br1	122.36(3)
$d_{Co1-Br2A}$	2.4805(6)	∠Br2B-Co1-Br1	102.8(2)
$d_{Co1-Br2B}$	2.797(8)		
		∠Br2A-Co1-P1	93.84(3)
		∠Br2B-Co1-P1	113.5(2)
		∠Br2A-Co1-P2	92.05(3)
		∠Br2B-Co1-P2	95.6(2)
		∠Br2B-Co1-P3	90.3(2)
		∠Br2A-Co1-P3	90.50(3)

Figure S23. Solid-state structure of {(μ-PP_2)Co}$_2$ (**3**). Hydrogen atoms are omitted for clarity.

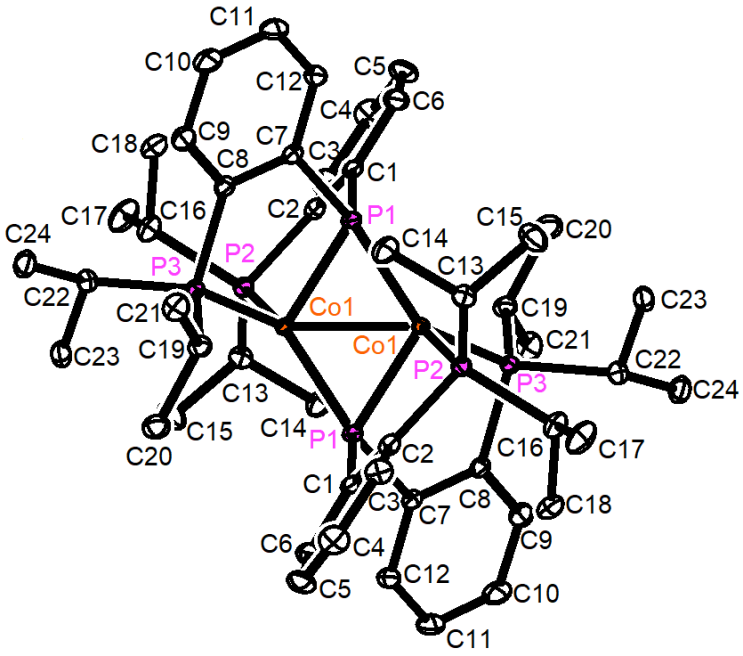

Table S3. Selected bond distances and angles for {(μ-PP_2)Co}$_2$ (Å and °).

Distance	{(μ-PP_2)Co}$_2$	Angle	{(μ-PP_2)Co}$_2$
		∠P1-Co1-P2	92.59(3)
$d_{Co1–Co1'}$	2.4118(8)	∠P1-Co1-P1'	112.39(3)
		∠P2-Co1-P1'	117.15(3)
$d_{Co1–P1}$	2.1454(8)	∠P1-Co1-P3	90.24(3)
$d_{Co1–P2}$	2.1887(8)	∠P2-Co1-P3	107.47(3)
$d_{Co1–P3}$	2.1926(9)	∠P1'-Co1-P3	127.80(3)
$d_{Co1–P1'}$	2.1888(8)	∠P1'-Co1-Co1'	55.34(2)
$d_{Co1'–P1}$	2.1889(8)	∠P3-Co1-Co1'	124.06(3)
$d_{P1'–P1}$	3.602(1)		

Figure S24. Solid-state structure of $(P_2P\text{-}PP_2)\{Co(OPh)\}_2$ (**1-OPh**). Hydrogen atoms are omitted for clarity.

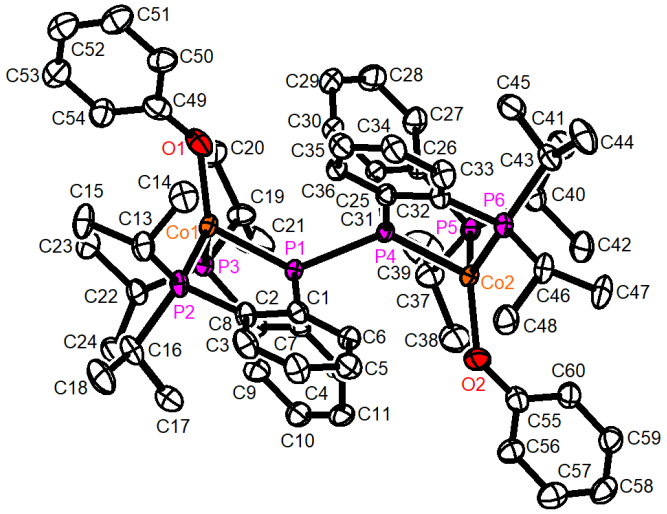

Table S4. Selected bond distances and angles for $(P_2P\text{-}PP_2)\{Co(OPh)\}_2$ (Å and °).

Distance	$(P_2P\text{-}PP_2)\{Co(OPh)\}_2$	Angle	$(P_2P\text{-}PP_2)\{Co(OPh)\}_2$
d_{Co1-O1}	1.9249(3)	∠P1-Co1-P2	86.116(6)
d_{Co1-P1}	2.1906(3)	∠P1-Co1-P3	85.868(6)
d_{Co1-P2}	2.2415(2)	∠P2-Co1-P3	115.602(6)
d_{Co1-P3}	2.2610(3)		
d_{Co2-O2}	1.9024(3)	∠O1-Co1-P1	122.833(9)
d_{Co2-P4}	2.1857(3)	∠O1-Co1-P2	115.091(8)
d_{Co2-P5}	2.2556(3)	∠O1-Co1-P3	122.464(7)
d_{Co2-P6}	2.2351(2)		
		∠P4-Co2-P5	86.130(6)
d_{P1-P4}	2.2638(3)	∠P4-Co2-P6	86.332(6)
		∠P5-Co1-P6	115.572(5)
		∠O2-Co2-P4	121.958(9)
		∠O2-Co2-P5	123.419(7)
		∠O2-Co1-P6	114.357(8)

Figure S25. Solid-state structure of ($PP^{OAr}P$)CoBr (**4-Br**) (Ar = 2,4,6-tri-*t*butylphenyl). Hydrogen atoms are omitted for clarity.

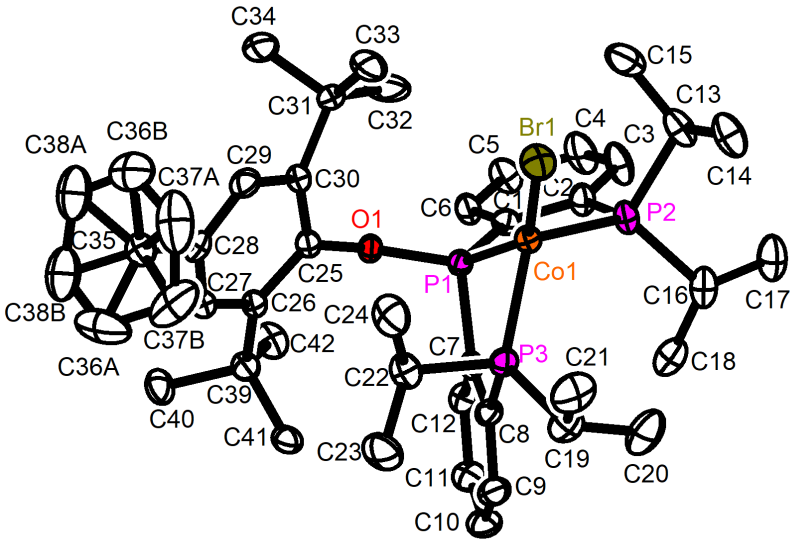

Table S5. Selected bond distances and angles for (PP^{OAr})CoBr (Å and °).

Distance	($PP^{OAr}P$)CoBr	Angle	($PP^{OAr}P$)CoBr
$d_{Co1–Br1}$	2.3772(8)	∠P1-Co1-P2	84.76(5)
$d_{Co1–P1}$	2.1924(1)	∠P1-Co1-P3	85.75(5)
$d_{Co1–P2}$	2.3012(1)	∠P2-Co1-P3	117.34(5)
$d_{Co1–P3}$	2.2763(1)		
$d_{P1–O1}$	1.684(3)	∠Br1-Co1-P1	144.84(4)
$d_{O1–C25}$	1.405(5)	∠Br1-Co1-P2	112.31(4)
		∠Br1-Co1-P3	110.29(4)
		∠Co1-P1-O1	137.10(1)
		∠P1-O1-C25	122.6(3)

Figure S26. Solid-state structure of ($PP^{OAr}P$)Co(OPh) (**4-OPh**) (Ar = 2,4,6-tri-*t*butylphenyl). Hydrogen atoms are omitted for clarity.

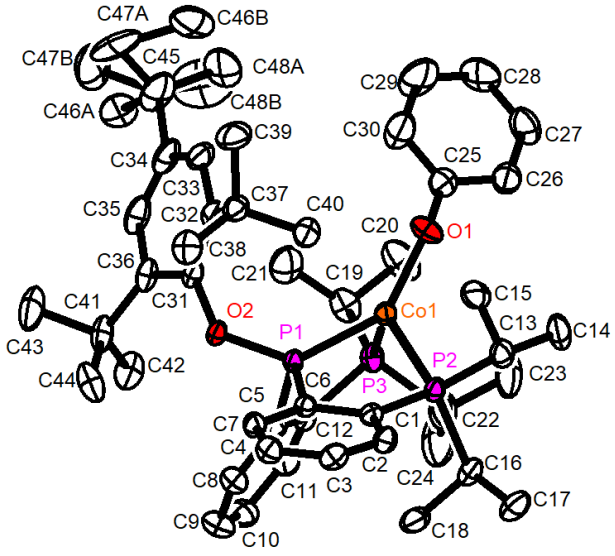

Table S6. Selected bond distances and angles for ($PP^{OAr}P$)Co(OPh) (Å and °).

Distance	($PP^{OAr}P$)Co(OPh)	Angle	($PP^{OAr}P$)Co(OPh)
d_{Co1-O1}	1.8965(2)	∠P1-Co1-P2	85.152(5)
d_{Co1-P1}	2.1735(2)	∠P1-Co1-P3	88.678(5)
d_{Co1-P2}	2.2654(2)	∠P2-Co1-P3	109.517(5)
d_{Co1-P3}	2.2411(2)		
d_{P1-O2}	1.6844(2)	∠O1-Co1-P1	117.784(6)
		∠O1-Co1-P2	138.341(6)
		∠O1-Co1-P3	111.835(6)
		∠Co1-P1-O1	134.535(7)

Figure S27. Solid-state structure of (PPP)Co(CN^{t}Bu)$_2$ (**5**). Hydrogen atoms are omitted for clarity.

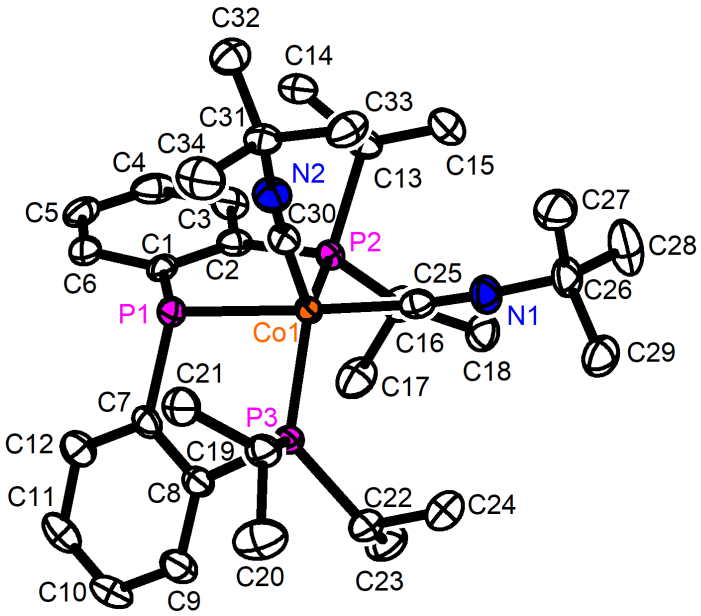

Table S7. Selected bond distances and angles for (PPP)Co(CN^{t}Bu)$_2$ (Å and °).

Distance	(PPP)Co(CN^{t}Bu)$_2$	Angle	(PPP)Co(CN^{t}Bu)$_2$
$d_{Co1–P1}$	2.2709(8)	∠P2-Co1-P3	130.20(3)
$d_{Co1–P2}$	2.1697(8)	∠P2-Co1-P1	86.49(3)
$d_{Co1–P3}$	2.1881(8)	∠P3-Co1-P1	84.96(3)
$d_{Co1–C25}$	1.823(3)	∠C30-Co1-P2	117.25(8)
$d_{Co1–C30}$	1.832(3)	∠C30-Co1-P3	111.61(8)
		∠C30-Co1-P1	89.33(8)
		∠C25-Co1-C30	88.13(1)
$d_{C25–N1}$	1.173(3)	∠C25-Co1-P2	94.01(8)
$d_{C30–N2}$	1.169(3)	∠C25-Co1-P3	96.68(8)
		∠C25-Co1-P1	177.35(8)
		∠Co1-C25-N1	174.7(2)
		∠Co1-C30-N2	176.7(2)

Figure S28. Solid-state structure of (PP^{OPh}P)Co(OPh) (**6**). Hydrogen atoms are omitted for clarity.

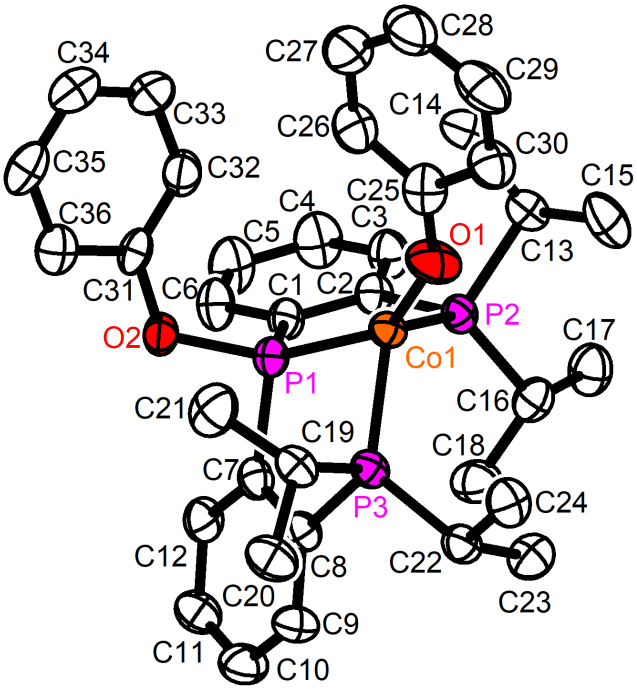

Table S8. Selected bond distances and angles for (PP^{OPh}P)Co(OPh) (Å and °).

Distance	(PP^{OPh}P)Co(OPh)	Angle	(PP^{OPh}P)Co(OPh)
d_{Co1-P1}	2.1506(1)	∠O1-Co1-P1	144.77(1)
d_{Co1-P2}	2.2623(1)	∠O1-Co1-P3	105.62(1)
d_{Co1-P3}	2.2504(1)	∠P1-Co1-P3	85.93(5)
d_{Co1-O1}	1.880(3)	∠O1-Co1-P2	116.17(1)
d_{Co1-O2}	1.679(3)	∠P1-Co1-P2	84.74(4)
		∠P3-Co1-P2	118.23(5)
d_{O1-C25}	1.257(5)	∠C25-O1-Co1	144.2(2)
d_{O2-C31}	1.383(5)	∠C31-O2-P1	119.6(2)

Figure S29. Solid-state structure of {(PPP)Co(CN^{t}Bu)}$_2$ (**7**). Hydrogen atoms are omitted for clarity.

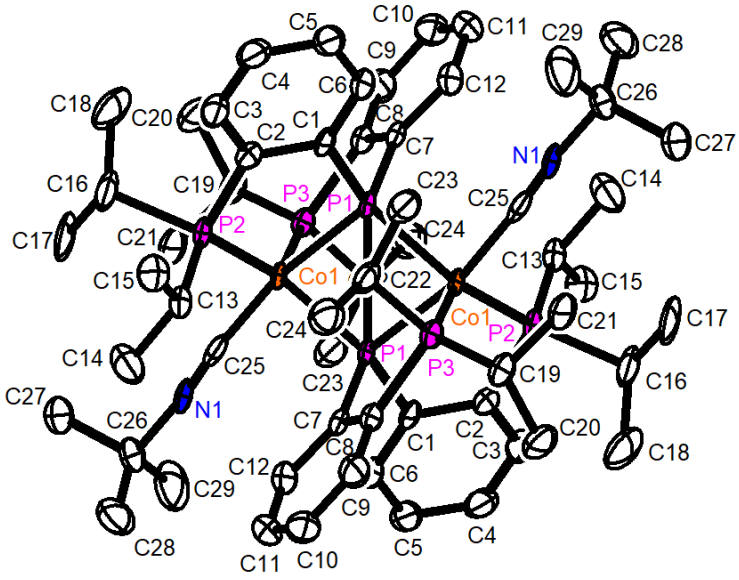

Table S9. Selected bond distances and angles for {(PPP)Co(CN^{t}Bu)}$_2$ (Å and °).

Distance	{(PPP)Co(CN^{t}Bu)}$_2$	Angle	{(PPP)Co(CN^{t}Bu)}$_2$
$d_{C25–N1}$	1.161(4)	∠P1-Co1-P1’	72.28(3)
$d_{Co1–C25}$	1.821(3)	∠P1-Co1-P2	117.00(3)
		∠P1’-Co1-P2	87.58(3)
$d_{Co1–P1}$	2.2321(9)	∠P1-Co1-P3	112.53(3)
$d_{Co1–P2}$	2.1860(9)	∠P1’-Co1-P3	87.97(3)
$d_{Co1–P3}$	2.1890(9)	∠P2-Co1-P3	126.00(4)
$d_{Co1–P1\$}$	2.2099(8)		
$d_{Co1–Co1’}$	3.5819(6)	∠C25-Co1-P1	95.28(1)
		∠C25-Co1-P1$	167.51(1)
		∠C25-Co1-P2	97.50(1)
		∠C25-Co1-P3	98.09(1)
$d_{P1–P1’}$	2.6197(2)	∠Co1-C25-N1	177.0(3)

Figure S30. UV-Vis spectra of (P_2P–PP_2)$(CoBr)_2$ (**1-Br**) (red), ($PP^{H}P$)$CoBr_2$ (green) and ($PP^{OAr}P$)CoBr (**4-Br**) (blue) in THF.

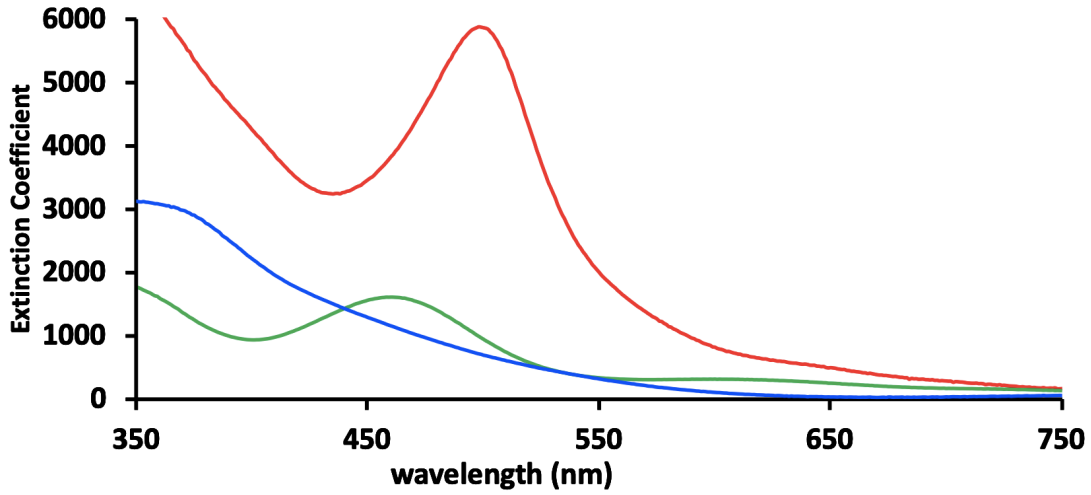

Figure S31. UV-Vis spectra of (P_2P–PP_2){Co(OPh)}$_2$ (**1-OPh**) (red) and ($PP^{OAr}P$)Co(OPh) (**4-OPh**) (blue) in THF.

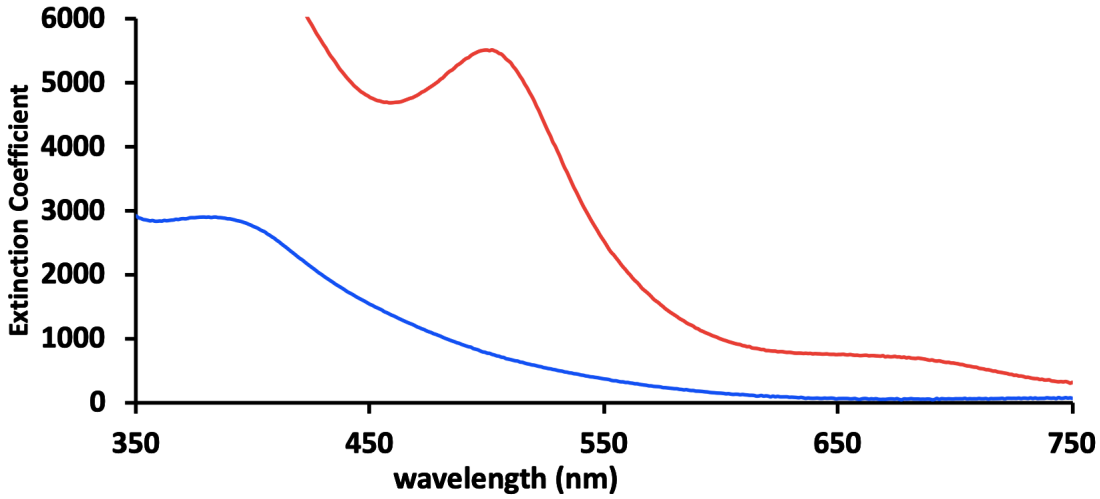

Figure S32. UV-Vis spectra of {(μ-PP_2)Co}$_2$ (**3**) (black), (PPP)$Co(CN^tBu)_2$ (**5**) (blue) and ($PP^{OPh}P$)Co(OPh) (**6**) (red) in THF.

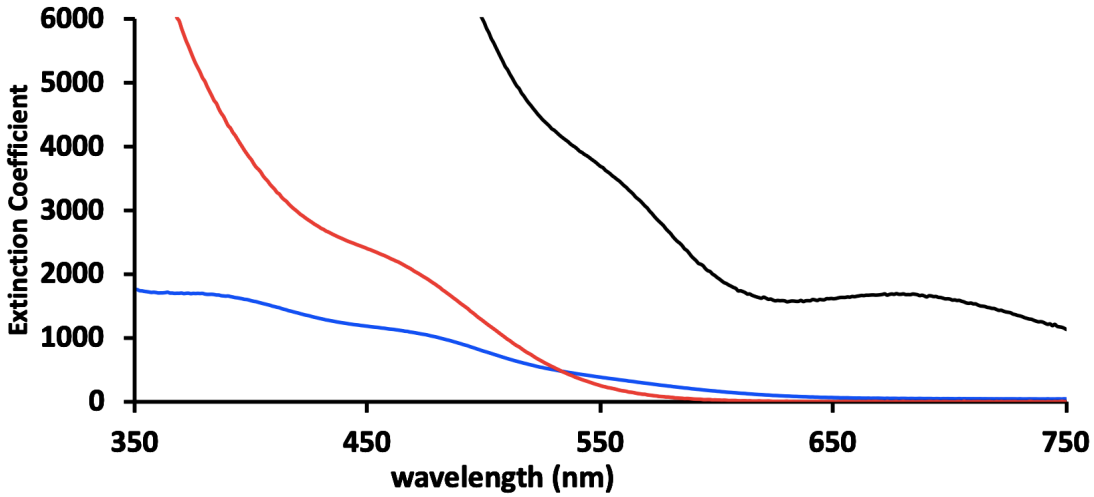

Figure S33. UV-Vis spectra of (P_2P–PP_2){$Co(OTf)$}$_2$ (**1-OTf**) (red) and {(PPP)$Co(CN^tBu)$}$_2$ (**7**) (blue) in THF.

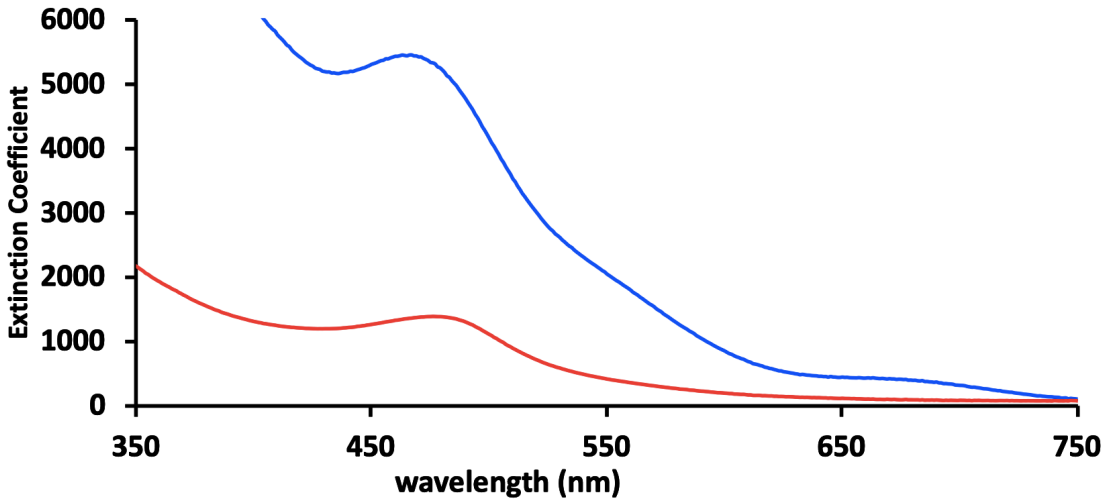

Figure S34. IR spectra of $PP^{H}P$ (black), $(P_2P–PP_2)(CoBr)_2$ (**1-Br**) (red) and $(PP^{H}P)CoBr_2$ (**2**) (green) (KBr pellet).

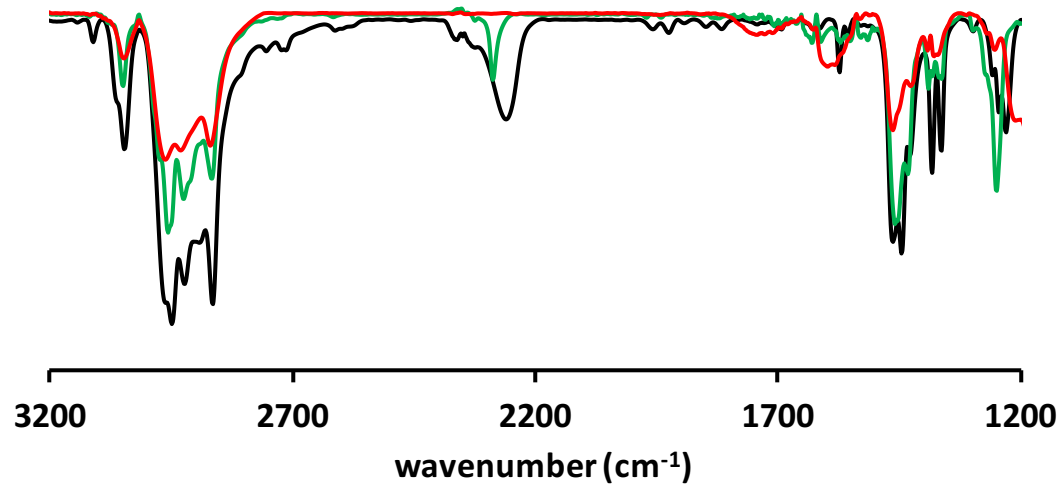

Figure S35. IR spectra of $(P_2P–PP_2)\{Co(OPh)\}_2$ (**1-OPh**) (black), $(PPP)Co(CN^tBu)_2$ (**5**) (red) and $(PP^{OPh}P)Co(OPh)$ (**6**) (blue) (KBr pellet).

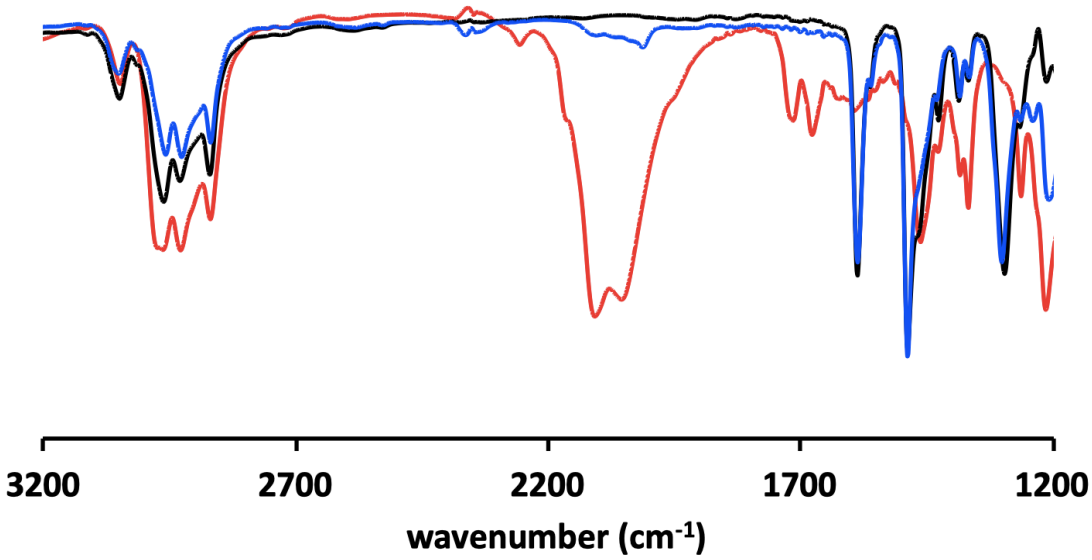

Figure S36. IR spectra of {(μ-PP_2)Co}$_2$ (**3**) (black) and {(PPP)Co(CN^{t}Bu)}$_2$ (**7**) (red) (KBr pellet).

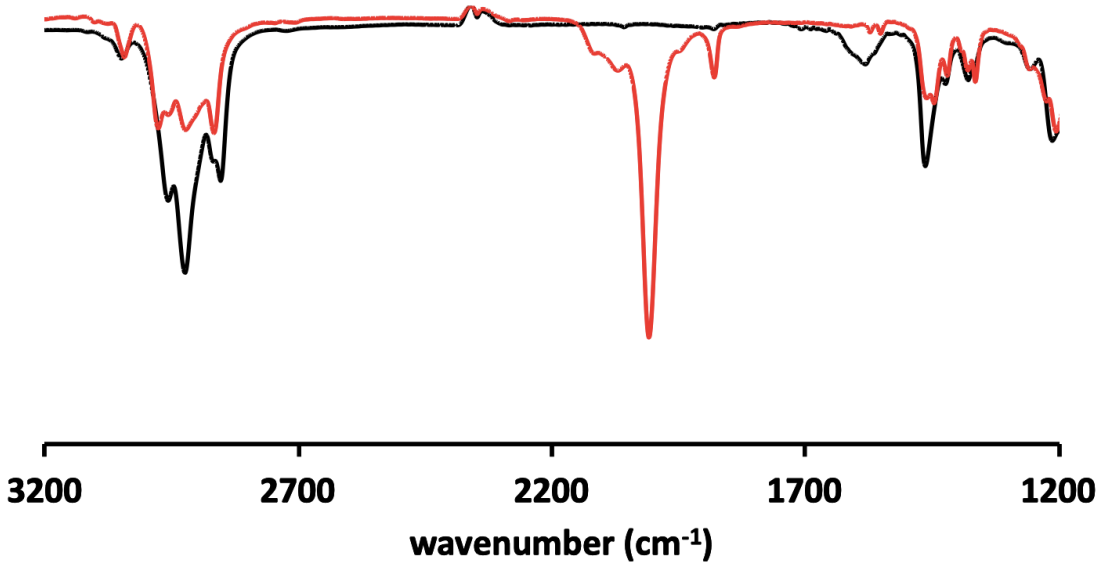

Figure S37. CSI mass data of {(PPP)Co(CNtBu)}$_2$ (**7**); blue bars represent calculated values and red bars represent experiment values.

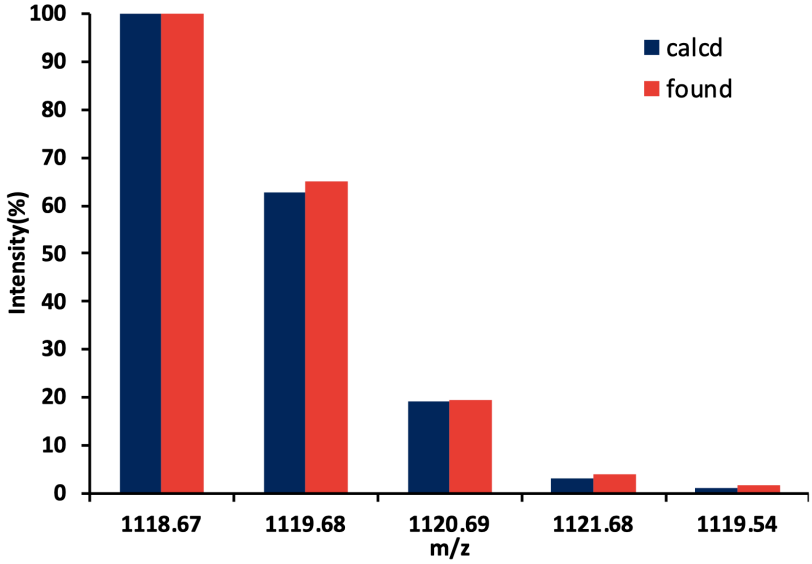

Figure S38. Cyclic voltammogram of {(P_2P-PP_2)CoBr}$_2$ (**1-Br**) with scan rates: 30, 40 and 50 mV/s. – 2.23 V vs. Fc/Fc^+ were observed in THF with 0.3 M tetra-*n*-butylammonium hexafluorophosphate as an electrolyte.

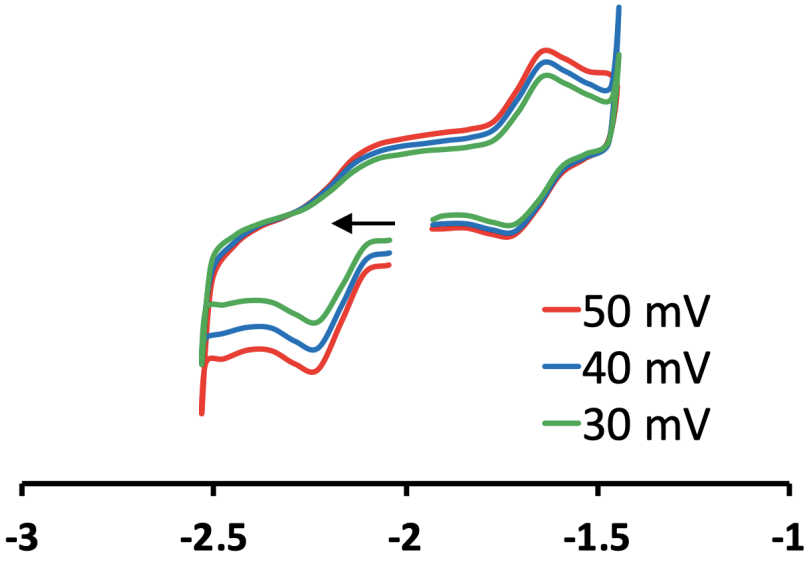

Figure S39. Electronic structures for (PPP)$CoBr_2$ derived from the single point DFT calculations; energies in cm^{-1}.

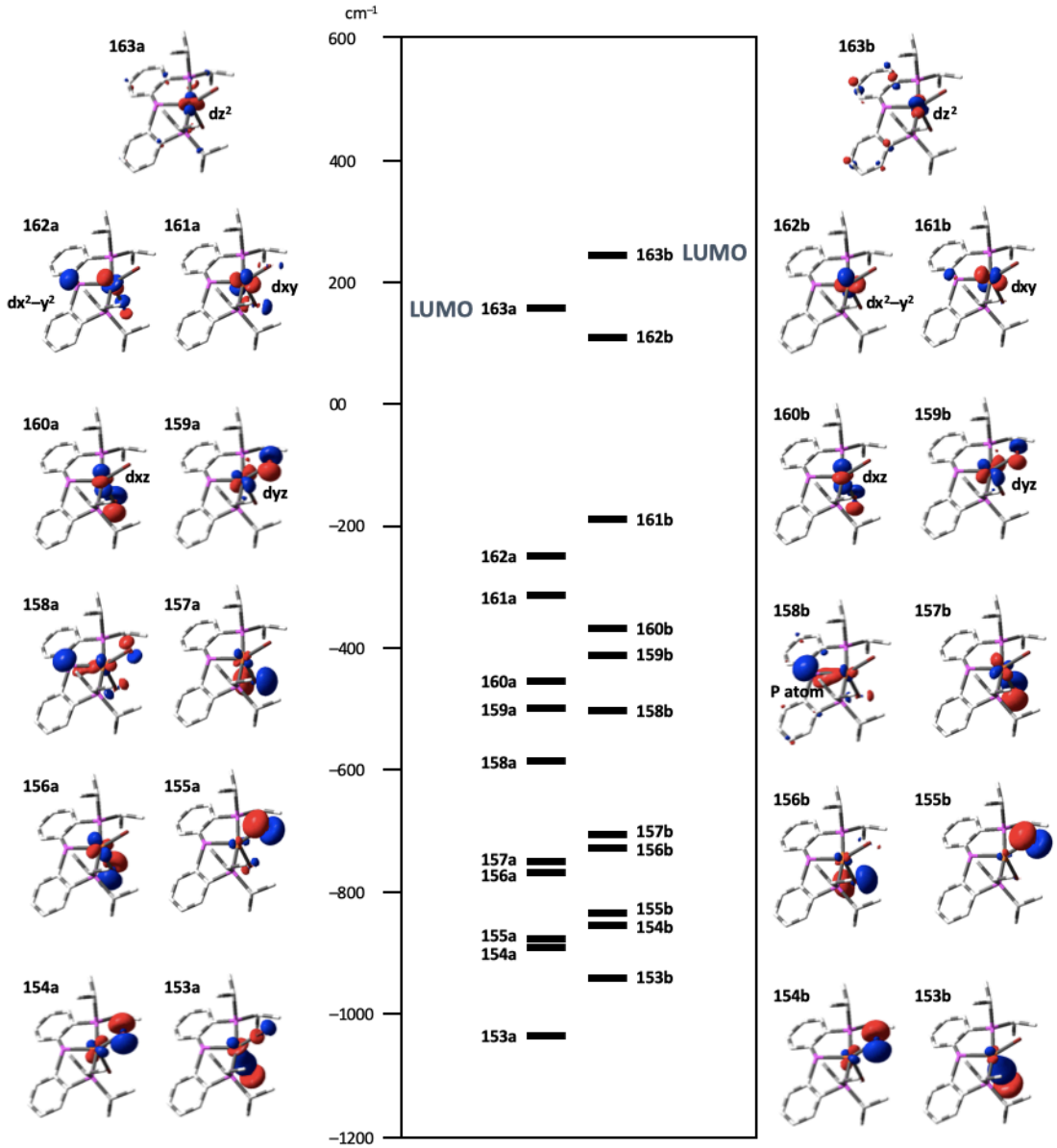

Figure S40. Electronic structures for (PPP)CoBr with S = 1/2 derived from the single point DFT calculations; energies in cm^{-1}.

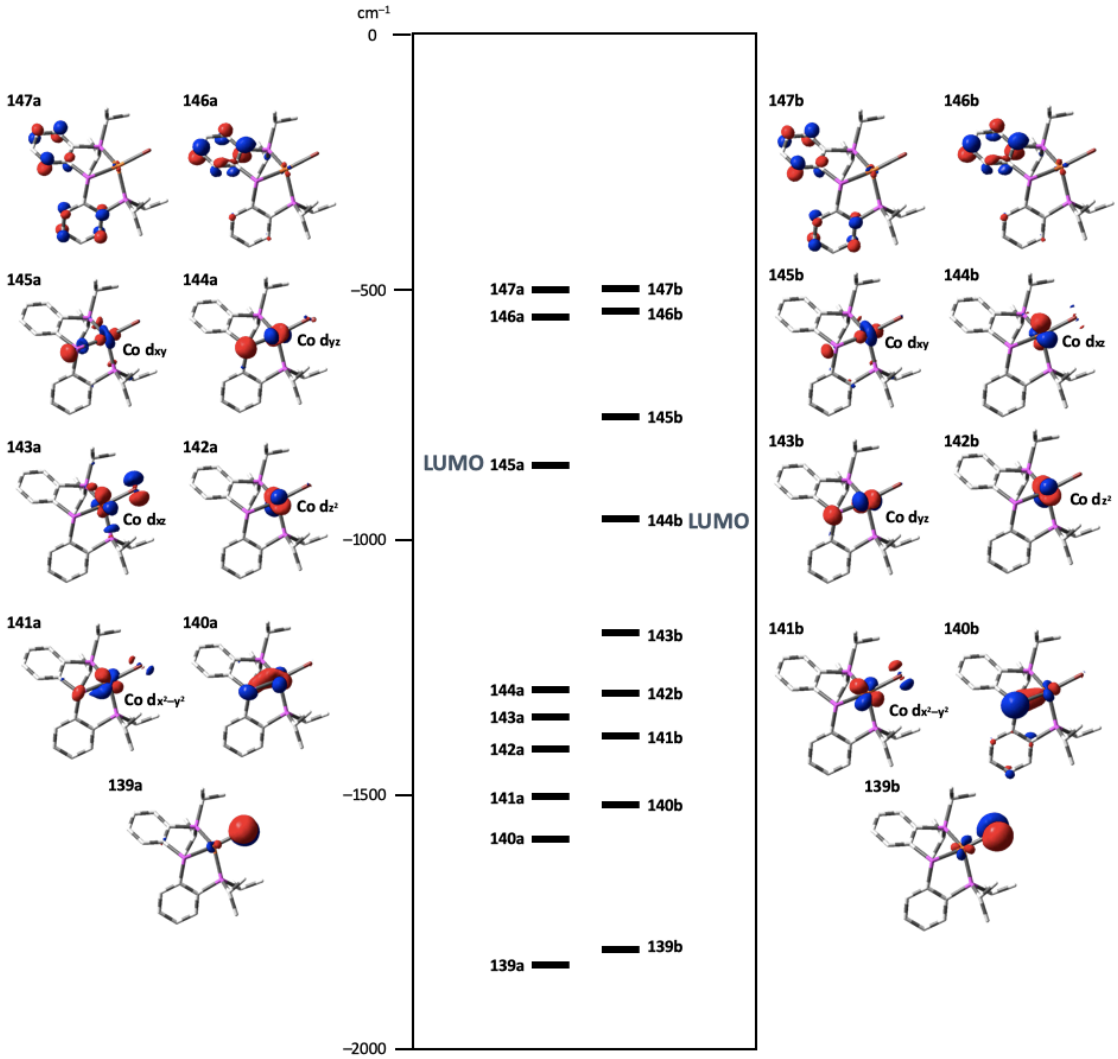

Figure S41. Electronic structures for (PPP)CoBr with S = 2/3 derived from the single point DFT calculations; energies in cm^{-1}.

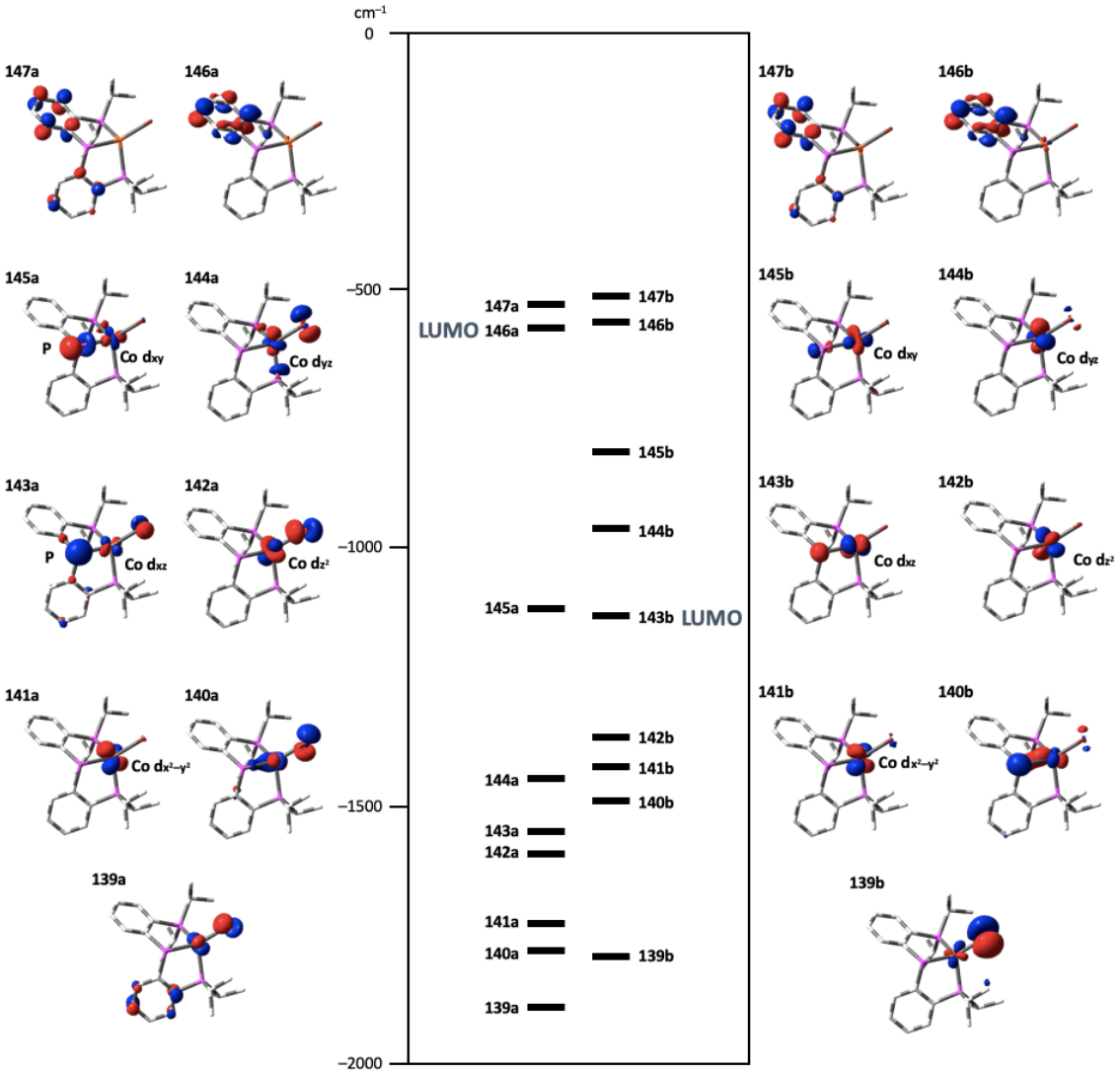

Figure S42. Electronic structures for $(P_2P\text{-}PP_2)(CoBr)_2$ (**1-Br**) derived from the single point DFT calculations; energies in cm^{-1}.

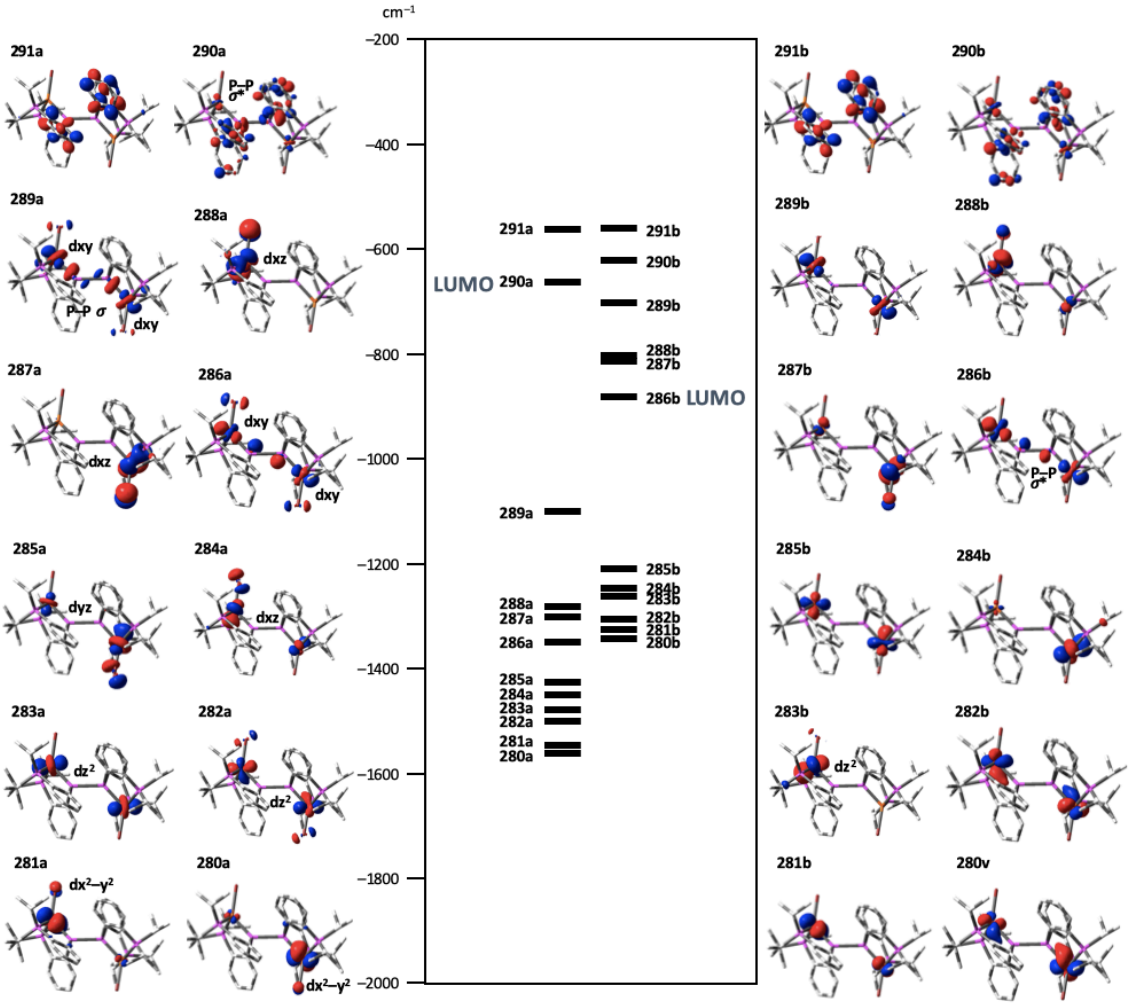

Figure S43. Electronic structures for {(μ-PP_2)Co}$_2$ (**3**) derived from the single point DFT calculations; energies in cm^{-1}.

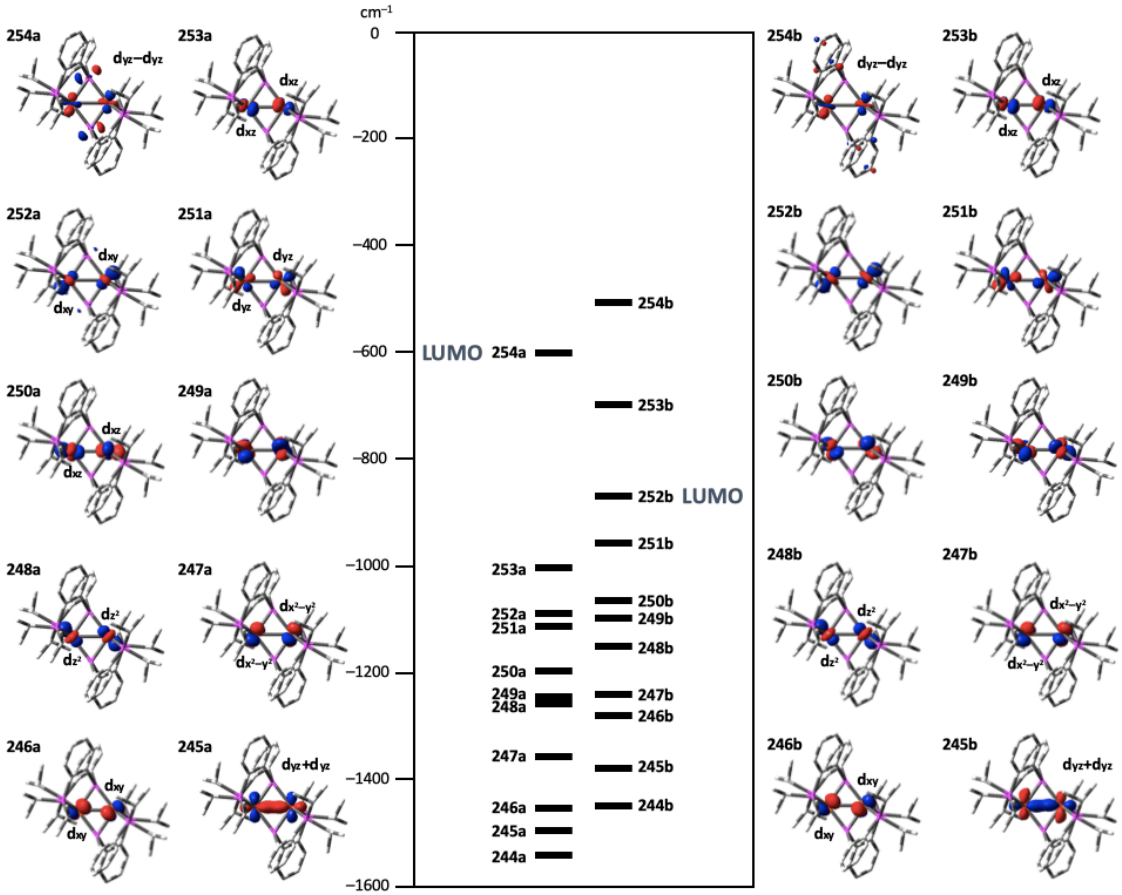

Figure S44. Mulliken atomic spin density plots derived from the single-point DFT calculations of (a) (PPP)$CoBr_2$, (b) (PPP)CoBr with $S = 1/2$ and (c) (PPP)CoBr with $S = 3/2$. Lobal representations to the spin density by the number with 0.004 isocontours.

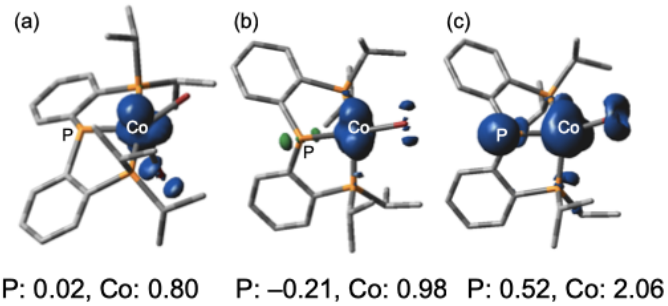

Figure S45. Optimized molecular structures for (PPP)CoBr with (a) $S = 1/2$ and (b) $S = 3/2$. Hydrogen atoms are omitted for clarity.

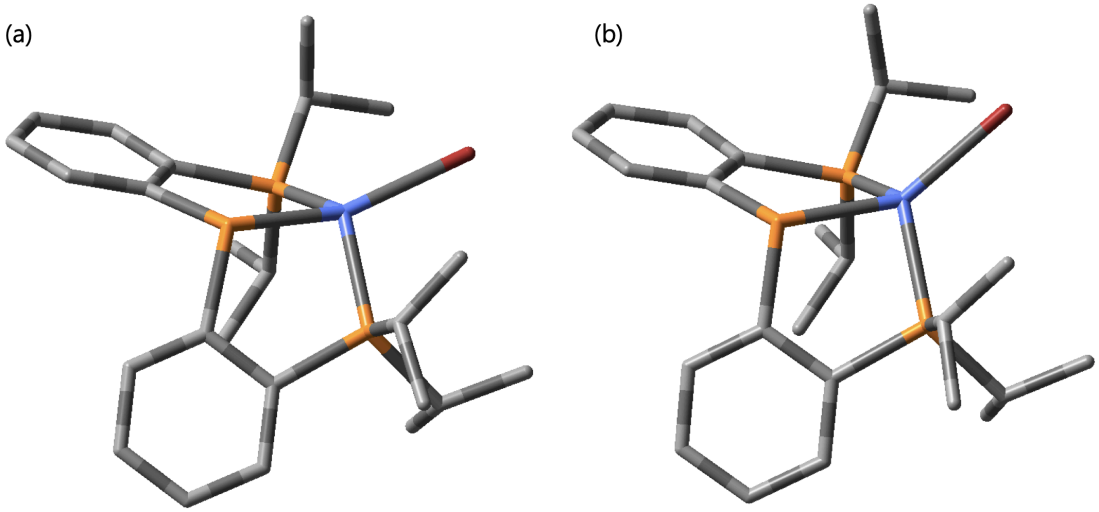

Table S10. Selected bond distances and angles for (PPP)CoBr with (a) $S = 1/2$ and (b) $S = 3/2$ of the calculated data based on the geometry optimization using DFT calculation.

Distance	$S = 1/2$	$S = 3/2$	Angle	$S = 1/2$	$S = 3/2$
$d_{Co–Br}$	2.33053	2.34872	∠P1-Co-P2 ∠P1-Co-P3 ∠P2-Co1-P3	86.929 83.983 127.473	86.500 84.825 122.614
$d_{Co1–P1}$ $d_{Co1–P2}$ $d_{Co1–P3}$	2.18485 2.22622 2.24080	2.25732 2.34254 2.31119	∠P1-Co-Br ∠P2-Co-Br ∠P3-Co-Br	152.327 107.066 104.422	137.685 110.909 113.156
			τ_4	0.57	0.71

Table S11. Computed energies (kcal mol^{-1}) of (PPP)CoBr and (P_2P-PP_2){CoBr}$_2$ (**1-Br**).

Complex	kcal mol^{-1}	ΔE (kcal mol^{-1})	Δ{(**1-Br**)–2(PPP)CoBr} (kcal mol^{-1})
(PPP)CoBr (S = 1/2)	–3711554.169	0	–1.173
(PPP)CoBr (S = 3/2)	–3711543.873	+10.296	+19.418
(P_2P–PP_2)(CoBr)$_2$ (S = 1)	–7423100.503	+6.662	–
(P_2P–PP_2)(CoBr)$_2$ (S = 2)	–7423107.165	0	0

Figure S46. LUMOs of (P_2P-PP_2){CoBr}$_2$ (**1-Br**) with S = 2.

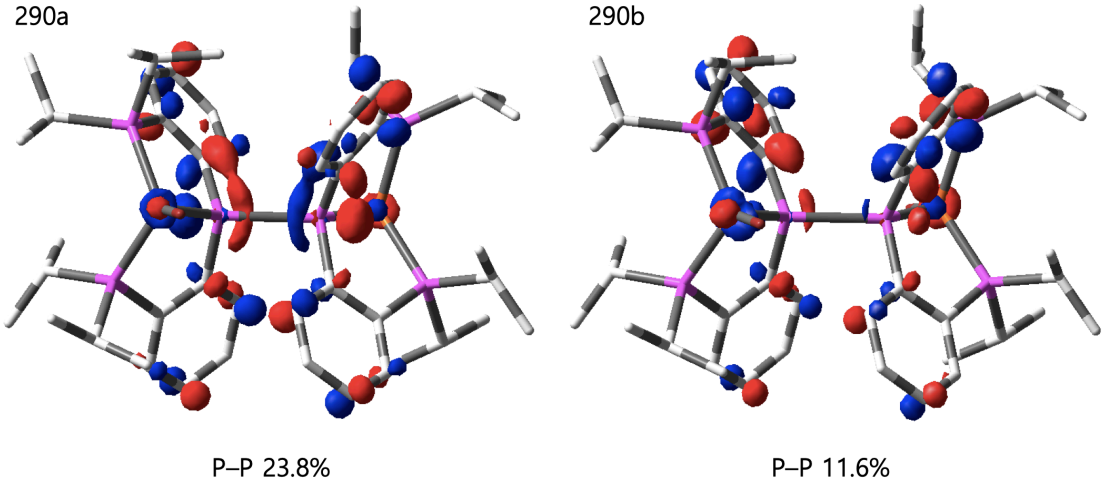

Figure S47. Mulliken atomic spin density plots derived from the single-point DFT calculations of (P_2P-PP_2){CoBr}$_2$ (**1-Br**) with S = 2. Lobal representations to the spin density by the number with 0.003 isocontours.

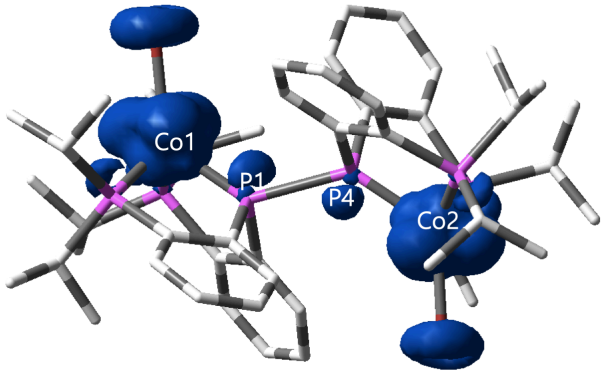

Co1 = 1.49 Co2 =1.52
P1 = 0.16 P4 = 0.14